Glycobiology, 2019, vol. 29, no. 1, 94–103
doi: 10.1093/glycob/cwy097
Advance Access Publication Date: 17 November 2018
Original Article

Structural Biology

Sequence-to-structure dependence of isolated IgG Fc complex biantennary *N*-glycans: a molecular dynamics study

Aoife M Harbison[2], Lorna P Brosnan[2], Keith Fenlon[2], and Elisa Fadda[2,3,1]

[2]Department of Chemistry and [3]Hamilton Institute, Maynooth University, Maynooth, Kildare, Ireland

[1]To whom correspondence should be addressed: Tel: +353 1 708 4616; e-mail: elisa.fadda@mu.ie

Received 29 August 2018; Revised 28 September 2018; Editorial decision 12 October 2018; Accepted 15 October 2018

Abstract

Fc glycosylation of human immunoglobulins G (IgGs) is essential for their structural integrity and activity. Interestingly, the specific nature of the Fc glycoforms is known to modulate the IgG effector function and inflammatory properties. Indeed, while core-fucosylation of IgG Fc-glycans greatly affects the antibody-dependent cell-mediated cytotoxicity function, with obvious repercussions in the design of therapeutic antibodies, sialylation can reverse the antibody inflammatory response, and galactosylation levels have been linked to aging, to the onset of inflammation, and to the predisposition to rheumatoid arthritis. Within the framework of a structure-to-function relationship, we have studied the role of the *N*-glycan sequence on its intrinsic conformational propensity. Here we report the results of a systematic study, based on extensive molecular dynamics simulations in excess of 62 μs of cumulative simulation time, on the effect of sequence on the structure and dynamics of increasingly larger, complex biantennary N-glycoforms isolated from the protein, i.e. from chitobiose to the larger *N*-glycan species commonly found in the Fc region of human IgGs. Our results show that while core fucosylation and sialylation do not affect the intrinsic dynamics of the unlinked *N*-glycans, galactosylation of the α(1–6) arm shifts dramatically its conformational equilibrium from an outstretched to a folded conformation. These findings are in agreement with and can help rationalize recent experimental evidence showing a differential recognition of positional isomers in glycan array data and also the preference of sialyltransferase for the more accessible, outstretched α(1–3) arm in both isolated, and Fc-bound *N*-glycans.

Key words: Fc-glycosylation, glycoinformatics, IgG, molecular dynamics, *N*-glycans

Introduction

N-glycosylation of the immunoglobulin G (IgG) fragment crystallizable (Fc) region is essential for its structural stability and function (Krapp, Mimura, et al. 2003; Arnold, Wormald, et al. 2007; Kobata 2008; Fang, Richardson, et al. 2016). The sequence and branching of the Fc N-glycoforms, bound at the highly conserved Asn 297 in both CH_2 domains of the Fc region, strongly affect the antibody-mediated effector function (Raju 2008; Subedi and Barb 2016; Hayes, Frostell, et al. 2017) by modulating the binding to the immune cells' Fc receptors, thus the antibody-mediated immune response (Tao and Morrison 1989; Shields, Namenuk, et al. 2001). In this context the effects of core-fucosylation, sialylation and galactosylation are particularly interesting. Between 81 and 98.7% of the Fc *N*-glycans in human IgGs are core-fucosylated (Pucic, Knezevic, et al. 2011). Core fucosylation, where fucose is α(1–6) linked to the chitobiose core, greatly affects the IgG antibody-dependent cell-mediated cytotoxicity (ADCC) function. More specifically, a strongly enhanced ADCC corresponds to nonfucosylated Fc *N*-glycan species (Satoh, Iida, et al. 2006; Kanda, Yamada, et al. 2007; Matsumiya, Yamaguchi, et al. 2007; Strohl 2009; Ratner

2014; Subedi and Barb 2016; Chen, Hsu, et al. 2017; Li, DiLillo, et al. 2017). This information has found wide interest and applications in cancer immunotherapy, especially in regards to the engineering of nonfucosylated antibodies with higher efficacy (Iida, Misaka, et al. 2006; Satoh, Iida, et al. 2006; Iida, Kuni-Kamochi, et al. 2009; Strohl 2009; Oflazoglu and Audoly 2010; Hayes, Frostell, et al. 2017). The molecular basis for this phenotype is not entirely clear. It has been linked to the stronger binding between IgG and the Fc γ receptor IIIa (FcγRIIIa) (Okazaki, Shoji-Hosaka, et al. 2004; Ferrara, Grau, et al. 2011; Hayes, Frostell, et al. 2017), determined by a more effective contact between the IgG and FcγRIIIa glycans in the absence of core fucose (Ferrara, Grau, et al. 2011). No significant structural changes in the IgG structure have been detected in function of the presence or absence of fucose (Matsumiya, Yamaguchi, et al. 2007). Sialylation of the Fc glycans is known to reverse the antibody inflammatory effect from pro to anti (Anthony, Nimmerjahn, et al. 2008). Only about 20% of core-fucosylated biantennary Fc *N*-glycans are sialylated (Pucic, Knezevic, et al. 2011), meanwhile the majority of Fc *N*-glycans in human IgGs are galactosylated, with neutral glycans without galactose slightly below 40%, neutral glycans with one terminal galactose slightly above 40%, and neutral glycans with two terminal galactoses contributing to 20% of the neutral IgG glycome (Pucic, Knezevic, et al. 2011). The abundance of galactosylated glycoforms has been directly linked to aging, with decreasing levels correlated with aging, and to immune activation (Parekh, Isenberg, et al. 1989; Pucic, Knezevic, et al. 2011; Karsten, Pandey, et al. 2012; de Jong, Selman, et al. 2016). Notably, the risk of developing rheumatoid arthritis is correlated with low levels of galactosylation (Parekh, Dwek, et al. 1985; Pasek, Duk, et al. 2006; Gudelj, Salo, et al. 2018).

The phenotypes linked to different Fc *N*-glycan sequences are likely to be determined by the modulation of the interaction of the IgG with cell surface receptors, which is a difficult topic to address as a whole due to the complexity and chemical diversity of the systems involved. NMR spin relaxation data provide evidence that despite the close contact with the protein, both arms of the *N*-glycans at the IgG Fc remain flexible and accessible (Barb and Prestegard 2011), suggesting that the intrinsic conformational propensity of the Fc *N*-glycan in function of its sequence may play a role in regulating the molecular interaction with the cell surface receptors. To understand the implications of size and sequence on the *N*-glycans structural and dynamics, we conducted a complete conformational study by extensive molecular dynamics (MD) simulations of progressively long complex biantennary Fc *N*-glycans most commonly expressed in human IgGs (Raju, Briggs, et al. 2000; Pucic, Knezevic, et al. 2011). All the glycoforms we have analyzed in this work are shown in Figure 1. Because of the complexity of the *N*-glycans dynamics and the high flexibility of α(1/2–6) linkages, we chose a sampling method based on single (conventional) MD trajectories, ran in parallel, all started from different combinations of α(1/2–6) rotamers, namely three trajectories for one α(1–6) linkage, 9 for two α(1–6) linkages, 12 for one α(1–6) and one α(2–6) linkages, 24 for two α(1–6) and one α(2–6) linkages, and finally 72 for two α(1–6) and two α(2–6) linkages, for a total cumulative sampling time in excess of 62 μs. This approach allowed us to systematically and directly "sample by construction" regions of the potential energy surface corresponding to rare conformations of the different α(1/2–6) linkages and to assess their relative stability. Our results show that (a) the highest conformational flexibility concerns primarily the α(1–6) arm, while the α(1–3) arm remains mostly extended, (b) core fucosylation and sialylation do not affect the conformational equilibrium of the α(1–6) arm in the isolated glycan in solution, meanwhile (c) galactosylation of the α(1–6) arm alone greatly shifts the conformational propensity of the arm from outstretched, to folded over the chitobiose core. These findings provide important insight into the differences in the molecular recognition of biantennary complex *N*-glycans by enzymes and lectins in function of their sequence. Implications in the molecular recognition of the different glycoforms studied here when isolated (unlinked), Fc-linked, and when on glycan arrays are discussed in the sections below.

Results

The results below are presented in function of the different *N*-glycan linkages for clarity. Notable effects on the conformational propensity of different linkages determined by the *N*-glycan size and sequence are indicated within. All torsion angles discussed throughout correspond to the following nomenclature, ϕ ($O_5C_1O_xC_x$), ψ ($C_1O_xC_xC_{x+1}$) and ω ($O_6C_6C_5C_4$) (Wormald, Petrescu, et al. 2002). The method we have chosen to number the monosaccharides and to name the different *N*-glycans is indicated in Figure 1. A summary of the results obtained as averages over all the simulations for all fucosylated and nonfucosylated species is shown in Tables I and II, respectively. Results obtained for each system studied are shown in Tables S4–S24.

GlcNAc(2)-β(1–4)-GlcNAc(1) linkage

As shown in Tables I and II, this linkage is conformationally rigid with only one rotamer populated in all the *N*-glycans analyzed. The average ϕ angle values are −78.7° and −77.9°, while the ψ angle values are −130.8° and −127.5° for nonfucosylated and for fucosylated species, respectively. In the core-fucosylated species this conformation of the chitobiose favors the formation of a hydrogen bond between the O2 of the fucose and the NH of GlcNAc(2). No significant deviations from these torsion angle values have been observed, except in the case of the core-fucosylated tetrasaccharide sugar D, shown in Figure 1, where the GlcNAc(1) ring pucker has been observed to transition from the more stable $^4C_1$ to a $^1C_4$ chair, causing a change to a ψ angle value of −74.0° for 13% of the time over a 3 μs trajectory. Because this transition has been seen exclusively for sugar D and it is caused by the reorientation of the GlcNAc(1) C5-C6 bond following the $^4C_1$ to $^1C_4$ repuckering, from an equatorial to an axial position, sugar D has been excluded from the averaging. The conformational propensity of sugar D is discussed in detail in a dedicated subsection below.

Fuc(12)-α(1–6)-GlcNAc(1) linkage

The flexibility of the α(1–6) linkage between the fucose and the GlcNAc(1) is unsurprisingly higher relative to the other core monosaccharides. Notably, the conformational space sampled is independent of the length or the size of the *N*-glycan. The highest populated α(1–6) conformer, i.e. ϕ −77.3°(100%), ψ −185.2°(78%) and ω 47.1° (89%), with relative average populations indicated in parentheses, corresponds to a structure where the fucose O2 forms a hydrogen bond with the NH of GlcNAc(2). An example of this conformation is shown in the case of the dodecasaccharide sugar T in Figure 2. As the size of the glycan increases the fucose is also able to extend the hydrogen bond network by forming interactions with the GlcNAc(7) O3 when the α(1–6) arm is folded over the chitobiose core, as shown in Figure 2. A deviation from this conformation with 19% of the total population, consistently for all *N*-glycans, has the

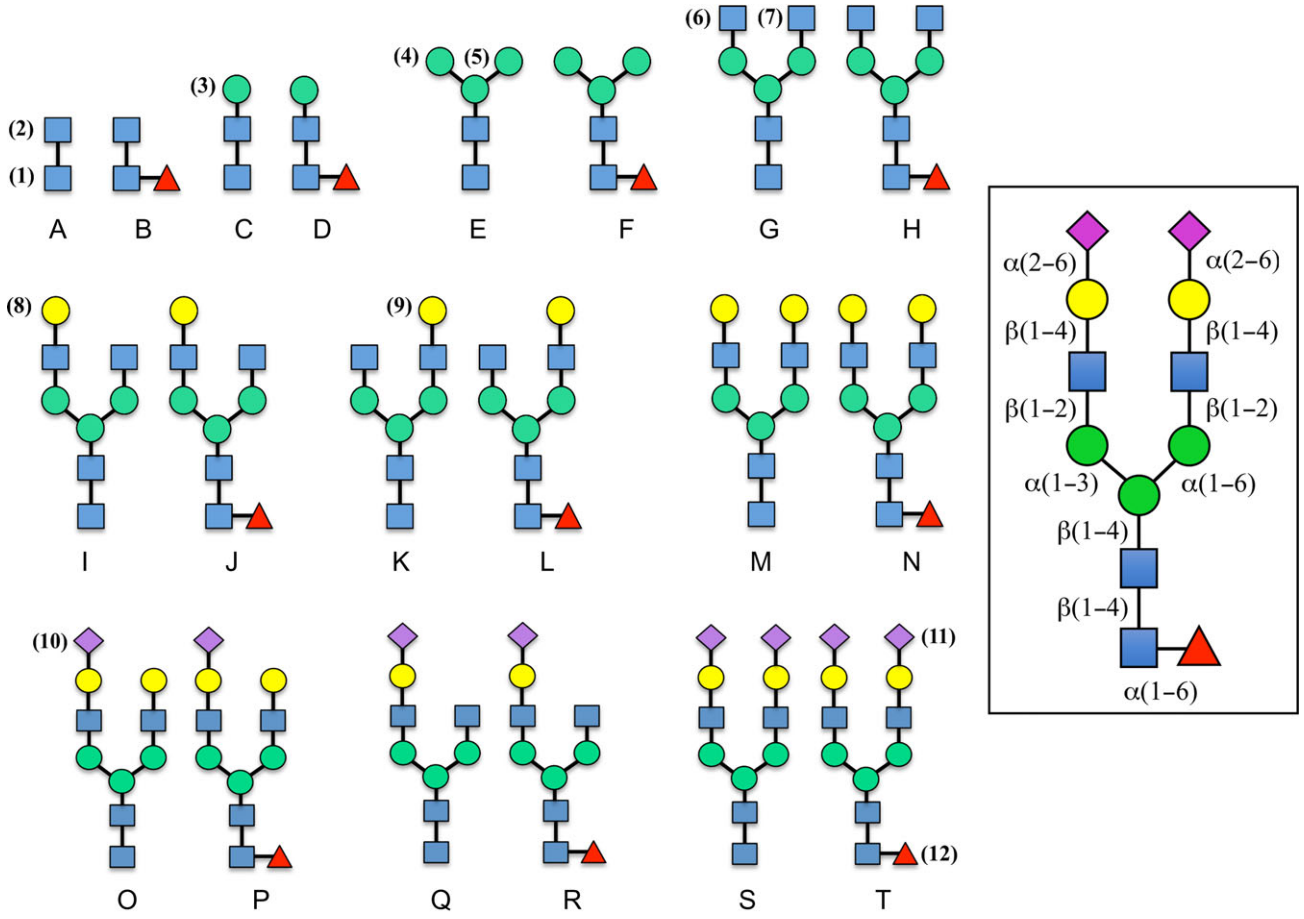

Fig. 1. Schematic representations of all *N*-glycans, fucosylated and nonfucosylated in pairs, analyzed in this study. Letters are used as shorthand notation for the identification of each sugar, numbers are used to identify residues and the conformation of the linkages is indicated on sugar T on the right hand side of the figure. The graphical representation follows the guidelines indicated in (Varki Cummings et al., 2015).

same ϕ and ω torsions, but a ψ value of 94.5°. In this conformer the fucose is not hydrogen bonded. A unique case where the ω torsion deviates from its *gg* stable configuration, i.e. ω of 47.1°, is found only in the case of the tetrasaccharide sugar D, where the reducing GlcNAc(1) $^{1}C_{4}$ chair conformation has the C5 in an axial positions and the ω torsion to adopt a −64.5° value. This ω value corresponds to an energetically prohibited *tg* conformer when the GlcNAc(1) is in the standard $^{4}C_{1}$ chair. The *gt* ω conformation, corresponding to an average value of −168.7°, has relative populations ranging between 3% (sugar T) and 15% (sugar F) in a pattern that does not seem to be dependent on the branching, the length, nor on the sequence.

Man(3)-β(1–4)-GlcNAc(2) linkage

This linkage has one largely preferred conformation for both, fucosylated and nonfucosylated species, irrespectively of the length and sequence of the *N*-glycan. For nonfucosylated species ϕ and ψ have average values of −79.6° (97%) and −125.4° (96%), respectively. The relative populations calculated over the entire simulation time are indicated in parentheses. For core-fucosylated species ϕ and ψ have average values of −78.1° (97%) and −125.5° (96%), respectively. Conformational changes from this prevalent configuration amount to 3–4% of the whole cumulative simulation time and represent changes of ϕ to values around −160° and of ψ to values around 60° for both, nonfucosylated and core-fucosylated species (Tables I and II). These ϕ and ψ excursions are not correlated to each other and confer a slight flexibility in terms of rotations of the plane containing the α(1–3) and α(1–6) branches around the chitobiose core. In the most stable conformation the planes containing the chitobiose and the trimannose core are parallel to each other.

α(1–3) branch: Man(4)-α(1–3)-Man(3) linkage

The conformational dynamics of the α(1–3) branch at the trimannose level is not particularly complex and it is not affected by core fucosylation. The ϕ torsion is prevalently found in a single conformation, 72.8° in 100% of all nonfucosylated species analyzed and 72.9° in 99% of all core-fucosylated species analyzed. The slight difference is due to the more complex dynamics of sugar P and sugar T, which both have sialylated α(1–3) arms, and for which in 5 and 1% of the sampling time the ϕ torsion value is an average of 123.7° (see Table S.10). The ψ torsion defines two distinct basins, identical in case of both fucosylated and nonfucosylated species. In case of nonfucosylated *N*-glycans the highest populated ψ value is 146.5° (61%) and the lowest is 102.3° (39%). In the case of fucosylated species the ψ values are, 147.5° with a relative population of 60% and 102.2 with a population of 39%. The remaining 1% is

Table I. Conformational propensities of different linkages calculated for all core-fucosylated species shown in Figure 1

Linkage	ϕ	ψ	ω
GlcNAc(2)-β(1–4)-GlcNAc(1)	−77.9 (11.3) 100	−127.5 (15.1) 100	–
Fuc(12)-α(1–6)-GlcNAc(1)	−77.3 (15.9) 100	−185.2 (19.5) 78/94.5 (19.4) 19/−97.3 (16.5) 2	47.1 (12.3) 92/−168.5 (16.5) 7/−54.8 (30.5) 1
Man(3)-β(1–4)-GlcNAc(2)	−78.1 (18.2) 97/−159.3 (18.5) 3	−125.5 (15.3) 96/72.1 (12.9) 4	–
(1–3) branch: Man(4)-α(1–3)-Man(3)	72.9 (12.2) 99/123.7 (22.0) 1	147.5 (15.2) 60/102.2 (14.5) 39	–
(1–3) branch: GlcNAc(6)-β(1–2)-Man(4)	−80.9 (16.5) 100	161.9 (15.6) 84/105.4 (12.4) 16	–
(1–3) branch: Gal(8)-β(1–4)-GlcNAc(6)	−75.1 (15.9) 100	−122.3 (16.5) 95/78.7 (21.2) 5	–
(1–3) branch: Sia(10)-α(2–6)-Gal(8)	65.1 (11.0) 90/−50.4 (15.2) 10	−182.6 (24.5) 85/−99.3 (16.7) 11/104.7 (17.9) 3	−63.7 (15.6) 64/−165.5 (15.0) 31/58.2 (14.3) 5
(1–6) branch: Man(5)-α(1–6)-Man(3) (F,H,J,R)	73.7 (15.8) 100	85.3 (17.2) 49/−178.5 (18.7) 50/−93.0 (17.4) 2	51.9 (10.7) 81/−173.6 (16.5) 15/−77.5 (19.6) 4
(1–6) branch: Man(5)-α(1–6)-Man(3) (L,N,P,T)	76.3 (15.0) 100	85.3 (15.8) 76/−185.1 (22.1) 23/−99.3 (13.6) 0	50.5 (9.8) 88/−172.8 (14.9) 11/−80.2 (18.1) 2
(1–6) branch: GlcNAc(7)-β(1–2)-Man(5)	−81.4 (14.9) 100	162.0 (13.1) 92/107.8 (11.8) 9	–
(1–6) branch: Gal(9)-β(1–4)-GlcNAc(7)	−74.8 (13.7) 100	−122.6 (15.7) 99/153.3 (9.1) 1	–
(1–6) branch: Sia(11)-α(2–6)-Gal(9)	64.9 (11.8) 88/−52.3 (19.1) 13	−182.0 (25.2) 88/−101.3 (16.6) 9/90.3 (16.3) 4	−64.9 (16.2) 56/−163.5 (15.2) 34/60.3 (14.4) 8

The torsion angle values are shown in degrees and calculated as averages over all *N*-glycans. Data were collected and analyzed at 100 ps intervals. Errors are shown in parenthesis and are averages of standard deviations calculated for each *N*-glycan. Relative populations (%) are indicated in red. All torsion angles discussed throughout correspond to the following nomenclature, ϕ (O5C1OxCx), ψ (C1OxCxCx+1) and ω (O6C6C5C4)

Table II. Conformational propensities of different linkages calculated for all nonfucosylated species shown in Figure 1

Linkage	ϕ	ψ	ω
GlcNAc(2)-β(1–4)-GlcNAc(1)	−78.7 (11.1) 100	−130.8 (15.7) 99/69.0 (12.4) 3	–
Man(3)-β(1–4)-GlcNAc(2)	−79.6 (20.6) 97/−157.9 (18.2) 1/56.7 (9.1) 1	−125.4 (15.4) 96/66.8 (11.8) 3	–
(1–3) branch: Man(4)-α(1–3)-Man(3)	72.8 (12.1) 100	146.5 (13.9) 61/102.3 (14.2) 39	–
(1–3) branch: GlcNAc(6)-β(1–2)-Man(4)	−81.0 (16.3) 100	161.8 (15.9) 84/105.4 (12.3) 16	–
(1–3) branch: Gal(8)-β(1–4)-GlcNAc(6)	−75.7 (17.3) 100	−122.1 (16.4) 95/74.5 (17.6) 5	–
(1–3) branch: Sia(10)-α(2–6)-Gal(8)	65.1 (11.2) 89/−50.0 (14.7) 11	−177.2 (22.9) 80/−100.3 (15.9) 18/105.9 (15.8) 3	−63.2 (15.5) 66/−164.3 (14.8) 31/60.3 (13.1) 4
(1–6) branch: Man(5)-α(1–6)-Man(3) (E,G,I,Q)	73.2 (16.5) 100	82.1 (18.4) 45/−177.7 (18.6) 54/−95.6 (17.7) 2	51.8 (11.0) 80/−172.3 (17.0) 15/−75.7 (17.9) 5
(1–6) branch: Man(5)-α(1–6)-Man(3) (K,M,O,S)	75.1 (14.9) 100	82.9 (17.3) 74/−182.2 (21.9) 26/−101.8 (13.4) 1	58.4 (10.3) 99/−173.5 (18.5) 1
(1–6) branch: GlcNAc(7)-β(1–2)-Man(5)	−79.8 (19.6) 100	162.1 (13.6) 90/106.5 (12.4) 10	–
(1–6) branch: Gal(9)-β(1–4)-GlcNAc(7)	−76.2 (15.1) 100	−125.7 (15.4) 97/120.3 (7.2) 3	–
(1–6) branch: Sia(11)-α(2–6)-Gal(9)	64.5 (11.2) 90/−50.7 (13.7) 10	−181.0 (25.2) 88/−98.6 (17.9) 9/106.5 (16.0) 3	−62.6 (15.6) 60/−66.6 (14.3) 33/58.8 (13.6) 7

The torsion angle values are shown in degrees and calculated as averages over all *N*-glycans. Data were collected and analyzed at 100 ps intervals. Errors are shown in parenthesis and are averages of standard deviations calculated for each *N*-glycan. Relative populations (%) are indicated in red. All torsion angles discussed throughout correspond to the following nomenclature, ϕ (O5C1OxCx), ψ (C1OxCxCx+1) and ω (O6C6C5C4)

contributed by the more complex dynamics of sugar P, where the third ψ value corresponds to 182.0°. The two distinct conformations of this linkage confer a degree of flexibility to the α(1–3) branch with a range of movement shown in Figure 3.

α(1–3) branch: GlcNAc(6)-β(1–2)-Man(4) linkage

The conformation of this linkage is restricted to two conformations, identical for both fucosylated and nonfucosylated species. In case of the nonfucosylated glycans the average ϕ value is −81.0°, while the

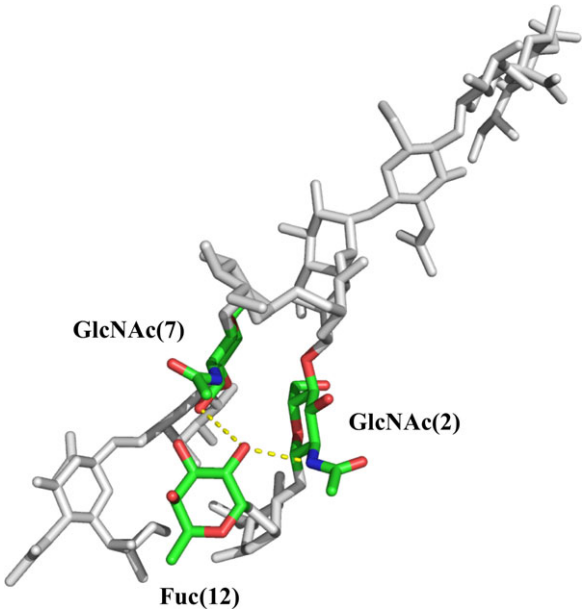

Fig. 2. Hydrogen bond between the Fuc(12) O2 and the amide N of GlcNAc(2) and GlcNAc(7) in the dodecasaccharide sugar T is highlighted with yellow dots. Aside from Fuc(12) and GlcNAc(2) all other monosaccharides are shown in light gray. Note: the conformation shown, the highest populated in sugar T, has the α(1–6) arm folded over the chitobiose core. The image was generated with pymol.

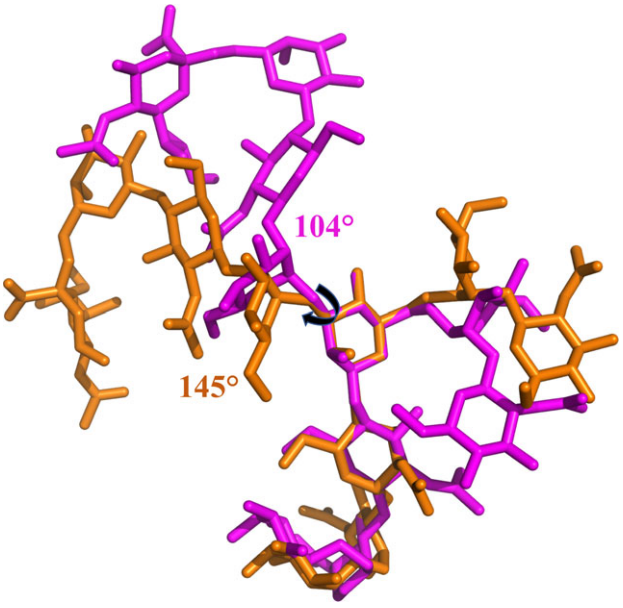

Fig. 3. The conformational dynamics of the α(1–3) arm, shown here for sugar R as an example, is restricted to two basins corresponding to ψ values of 145° (orange) and 104° (purple). The image was generated with pymol.

ψ values are 161.8° (84%) and 105.4° (16%). In case of the fucosylated glycans the average ϕ value is −80.9°, while the ψ values are 161.9° (84%) and 105.4° (16%).

α(1–3) branch: Gal(8)-β(1–4)-GlcNAc(6) linkage

This linkage is the least flexible in the branch with one conformation accounting for over 95% of the population of both fucosylated and nonfucosylated *N*-glycans. In case of the nonfucosylated glycans the average ϕ value is −75.7°, while the ψ value is −122.1°(95%). In case of the fucosylated glycans the average ϕ value is −75.1°, while the ψ value is −122.3°(95%). The 5% difference corresponds to excursions to ψ values around 75° for both fucosylated and nonfucosylated species (Tables I and II).

α(1–3) branch: Sia(10)-α(2–6)-Gal(8) linkage

The linkage to the terminal sialic acid is the most flexible of the α(1–3) arm and all the conformations visited are independent of core-fucosylation, both in terms of torsion angle values and populations (Tables I and II). The most flexible torsion is the ω angle with values around −60°(65%) and −165°(30%). A small contribution of around 5% is given by a value of 60°. These two ω values define the conformations shown in Figure 4, with the highest populated corresponding to the completely outstretched α(1–3) arm.

α(1–6) branch: Man(5)-α(1–6)-Man(3) linkage

The conformational dynamics of the Man(5)-α(1–6)-Man(3) linkage is the most interesting and the only one that has a clear dependence on sequence among the IgG Fc *N*-glycans analyzed in this work. Unlike the α(1–3) arm that has a relatively restricted dynamics, the α(1–6) arm can adopt two very distinct conformations, one extended, or "outstretched", corresponding to ϕ values around

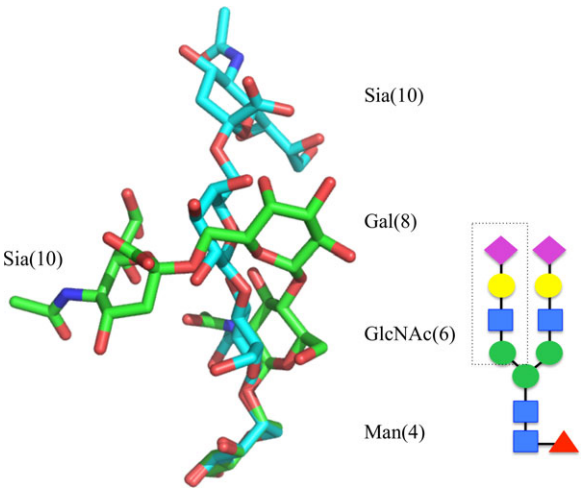

Fig. 4. The two highest populated conformations accessible to the terminal sialic acid here shown for sugar T on the α(1–3) arm. Note, only the section of the α(1–3) arm from Man(4) is shown for clarity. The conformations corresponding to ω torsion values of −60°(65%) and −165°(30%) are shown with C atoms in cyan and green, respectively. The image was generated with pymol.

−180°, and one where the arm is folded over the chitobiose core, which we will refer to as "folded-over", corresponding to ϕ values around 80° (Tables I and II and Figure 5). In sugar E (F), with an α(1–6) arm terminating with Man, over 80% of the conformers have the arm in an outstretched conformation (see Tables S17 and S18). The addition of the GlcNAc in β(1–2) shifts this equilibrium, so for sugars G (H), I (J) and Q (R), where the fucosylated species are indicated in parenthesis, the outstretched and the folded-over conformations are equally populated, namely 45% (49%) for the folded-over conformation, and 55% (51%) for the outstretched conformation. Interestingly, galactosylation of the α(1–6) arm shifts this

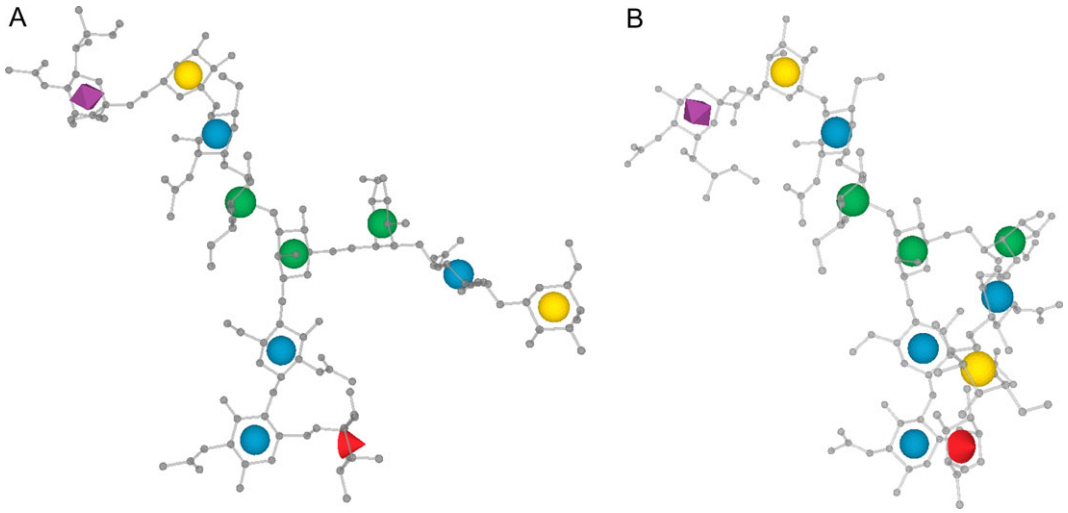

Fig. 5. Two main conformations accessible to the α(1–6) arm represented for sugar P as an example. The "outstretched" conformation is shown in panel (**A**) and the "folded-over" on panel (**B**). The image was generated with LiteMol with the 3D-SNFG rendering (Sehnal, Deshpande, et al. 2017).

equilibrium further with a high majority of the galactosylated sugars, namely K (L), M (N), O (P) and S (T), in a folded-over conformation. The relative average populations are 74 and 76% in a folded-over conformation for nonfucosylated and core-fucosylated sugars, respectively, while 26 and 23% in an outstretched conformation for nonfucosylated and core-fucosylated sugars, respectively. This equilibrium is not affected either by the type of glycosylation in the α(1–3) arm, nor by the sialylation of the α(1–6) arm, and it does not depend on core-fucosylation either, despite the fucose in its most stable conformation interacts effectively through hydrogen bonding with the α(1–6) arm when folded-over, as shown in Figure 2.

α(1–6) branch: GlcNAc(7)-β(1–2)-Man(5) linkage

As seen in the case of the α(1–3) arm, the conformational dynamics of this linkage is largely restricted to ϕ and ψ values of −80° and 162°, respectively, both in case of fucosylated and nonfucosylated species (Tables I and II). The only significant alternative conformer accounting for 10% total contribution is characterized by ψ values of 106° for nonfucosylated species and 108° for fucosylated species. The same linkage on the α(1–3) arm has an analogous conformational equilibrium of the ψ torsion, with a 85:15 ratio.

α(1–6) branch: Gal(9)-β(1–4)-GlcNAc(7) linkage

Similarly to the same linkage on the α(1–3) arm, the Gal(9)-β(1–4)-GlcNAc(7) torsional space is highly restricted to a single conformation with ϕ and ψ values around −75° and −125°, respectively, both in the cases of fucosylated and nonfucosylated species.

α(1–6) branch: Sia(11)-α(2–6)-Gal(9) linkage

The conformational dynamics of the terminal sialic acid on the α(1–6) arm is virtually identical to the one observed for the terminal sialic acid on the α(1–3) arm. The linkage is highly flexible with, the ϕ angle predominantly around 65°(90%), with a ~10% contribution of −52°. The ψ angle has also a preferred conformation around −180°(88%). Small contributions of ψ values around −100°(9%), and +100° (3–4%) have been also detected, both in case of fucosylated and of nonfucosylated species. The ω angle is quite flexible, with values of −65° as the preferred conformation (60%) and of −162°(33%). A small contribution of 7% corresponds to an ω value of 60°, both in case of fucosylated and of nonfucosylated species.

Sugar D: Man-β(1–4)-GlcNAc-β(1–4)-[α(1–6)-Fuc]-GlcNAc

The conformational dynamics of the tetrasaccharide Man-β(1–4)-GlcNAc-β(1–4)-[α(1–6)-Fuc]-GlcNAc, named here sugar D for short (Figure 1), is quite complex showing occasional transitions of the reducing GlcNAc ring from the stable $^4C_1$ chair conformation to a less stable $^1C_4$ chair. Similar conformational changes have been reported recently for Lewis X (Le^x) and sialyl Le^x (sLe^x) (Topin, Lelimousin, et al. 2016; Alibay, Burusco, et al. 2018), where the linkage to the fucose is a less flexible β(1–3). Although we observed the first $^4C_1$ to $^1C_4$ chair transition within the first 100 ns of the simulation, we extended the trajectory to 3 μs to evaluate more accurately the relative populations of the two different conformers. During the 3 μs trajectory the $^1C_4$ chair conformation is visited five times and remains stable during intervals ranging from 30 ns up to 200 ns. Based on these data, as shown in Figure 6, sugar D is found in the stable $^4C_1$ chair for over 87% of the time. In terms of relative populations, the corresponding free energy for the $^4C_1$ to $^1C_4$ chair transition corresponds to 4.7 kJ/mol at 300 K.

Discussion

The sequence of the *N*-glycans expressed at Asn 297 has been shown to have a significant effect in modulating the IgG effector function. In particular core-fucosylation, and galactosylation and sialylation of both α(1–6) and α(1–3) arms in Fc biantennary complex *N*-glycans have been identified as key players, with different roles in regulating the ADCC function (Satoh, Iida, et al. 2006; Raju 2008; Li, DiLillo, et al. 2017) and the onset of inflammation (Karsten, Pandey, et al. 2012; de Jong, Selman, et al. 2016). In particular levels of galactosylation have been linked to aging (Raju, Briggs, et al. 2000) and to the risk of developing conditions such as rheumatoid arthritis (Parekh, Dwek, et al. 1985; Parekh, Isenberg, et al. 1989; Pasek, Duk, et al. 2006; Gudelj, Salo, et al. 2018). The

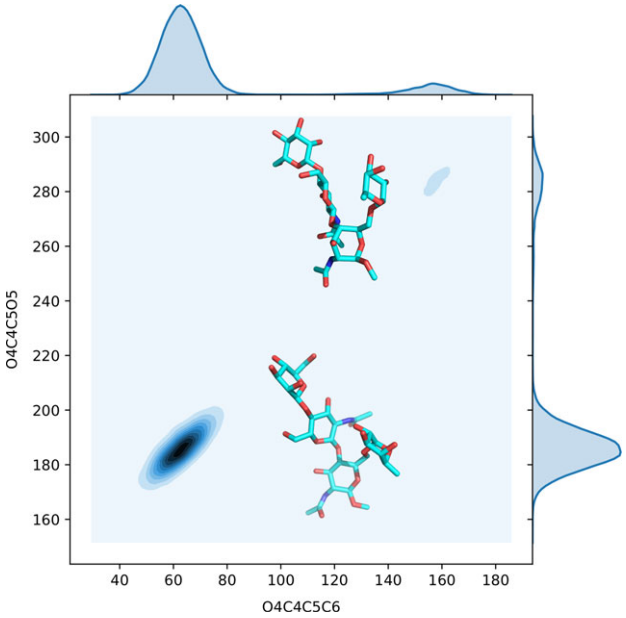

Fig. 6. Contour plot showing the conformational propensity of the reducing GlcNAc(1) of sugar D in function of two torsion angles O4C4C5C6 and O4C4C5O5 on the *x* and *y* axis, respectively. The structures corresponding to the highest populated $^4C_1$ chair conformation (87%) and the lowest populated $^1C_4$ chair conformation (13%) over 3 μs (30,000 data points) are also shown in line with the corresponding histograms on the *y* axis. Torsion angles are in degrees. 2D contour plots are done with seaborn (*seaborn.pydata.org*) and the structures are rendered with pymol.

molecular basis underlying the link between the glycan sequence and these different phenotypes is very complex to understand, as it most likely depends on the dynamics and energetics of the interaction between the glycosylated antibody and the receptors on the immune cells (Ferrara, Grau, et al. 2011). Our overarching project is to understand the molecular basis of such phenotypes, thus as a first step we determined if and how the monosaccharide sequence affects the *N*-glycan dynamics in the absence of the protein. To do so, we analyzed the intrinsic conformational propensity of the biantennary complex *N*-glycans most commonly expressed at Asn 297 on the IgG Fc (Raju 2008; Pucic, Knezevic, et al. 2011). Although we do expect that contacts with residues on the IgG Fc surface are likely to affect the conformational equilibrium relative to the isolated glycan, it has been shown that both α(1–6) and α(1–3) arms retain high degrees of flexibility in Fc-linked glycans (Barb and Prestegard 2011), therefore their intrinsic conformational propensity may play a role in their contact with the receptors. The results of our study show that while core-fucosylation and sialylation do not affect the conformational dynamics of the *N*-glycan as a whole, the effect of galactosylation of the α(1–6) arm is remarkable. Indeed, we have found that regardless of the sequence of the α(1–3) arm, of core-fucosylation, or of sialylation of the α(1–6) arm, the presence of β(1–4) galactose shifts the conformational propensity of the whole α(1–6) arm from an "outstretched" conformation to a "folded-over" conformation, where the α(1–6) arm is stacked against the chitobiose core (Figures 2 and 5). This shift in conformational equilibrium is likely due to a more effective interaction in terms of both hydrogen bonding, and of stacking, as shown in Figure 2. Surprisingly, despite the direct involvement of the core fucose in the hydrogen bonding network, the conformational shift of the α(1–6) arm depends exclusively on galactosylation. The dynamics of the α(1–3) arm is more restricted due to the intrinsic rigidity of the Man-α(1–3)-Man relative to the Man-α(1–6)-Man, with only small excursions between the two close rotamers, as shown in Figure 3. The conformational dynamics of both arms is locally enhanced by the sialic acid due to the intrinsic flexibility of the α(2–6) linkage.

Although the existence of folded-over (and variation there-of) and of outstretched conformations of the α(1–6) arm have been identified and discussed previously (Canales, Mallagaray, et al. 2013; Jo, Qi, et al. 2016; Galvelis, Re, et al. 2017), our systematic study highlights the unique dependence of this conformational propensity on the galactosylation of the α(1–6) arm. This behavior can explain the recent evidence of differential recognition of positional isomers in glycan array screening (Echeverria, Serna, et al. 2018). As an example, the positional isomers sugar J and L are galactosylated on the α(1–3) only, or on the α(1–6) arm only, respectively, which based on our data determines different conformational propensities. Indeed, in sugar J, shown in Figure 7A, the folded-over and the outstretched conformations are equally populated during the MD simulations, i.e. 49 and 50%, respectively (note: the 1% corresponds to a ψ value of −99.3°), while in sugar L, shown in Figure 7B, the folded-over α(1–6) arm is the dominant conformation with a relative population of 81% over the simulation time. As a further implication of this behavior, a different structural propensity shifted towards a folded-over α(1–6) arm and an outstretched α(1–3) arm is in agreement with the higher affinity of the sialyltransferase for the α(1–3) galactose, more accessible in isolated glycans (Barb, Brady, et al. 2009; Barb and Prestegard 2011; van den Eijnden, et al. 1980). Interestingly, this selectivity is only moderately changed when the *N*-glycans are linked to the IgG Fc (Barb and Prestegard 2011). The molecular basis for the preferential targeting of the α(1–3) arm in both isolated, and Fc-linked *N*-glycans can be very different though. Indeed, Fc-linked *N*-glycans are sterically confined and are known to interact extensively the protein surface (Barb and Prestegard 2011; Jo, Lee, et al. 2013; Lee and Im 2017). This interaction is highly likely to shift the α(1–6) arm conformational equilibrium. A search of structural data on the glycan fragment database (GFDB) (Jo and Im 2013), resulted in 17 structures containing core-fucosylated glycans that we have studied here in their isolated/unlinked form (see Table S.25). In all 17 structures the *N*-glycans have an outstretched conformation of the α(1–6) arm.

The systematic conformational analysis of progressively longer fucosylated and nonfucosylated *N*-glycans has allowed us to highlight an additional and unique complexity in the dynamics of the tetrasaccharide sugar D, namely Man-β(1–4)-GlcNAc-β(1–4)-[α(1–6)-Fuc]-GlcNAc. During a single (unbiased) MD trajectory extended to 3 μs, we have observed the reducing GlcNAc ring transitioning from the most stable $^4C_1$ chair to a $^1C_4$ chair a total of five times, where the $^1C_4$ chair remains stable for intervals between 30 and 200 ns. This relative ease of interconversion, corresponding to a free energy of 4.7 kJ/mol, is somewhat in contrast with the results obtained for of $Le^{x(a)}$ and $sLe^{x(a)}$ where opening events are much more rare and much more difficult to sample through conventional MD simulations (Topin, Lelimousin, et al. 2016; Alibay, Burusco, et al. 2018). The greater accessibility of the open state in sugar D is most likely related to the higher flexibility of the α(1–6) linkage to the fucose, relative to the α(1–3) and α(1–4) linkages in (s)Le^x and (s)Le^a, respectively. Indeed, in each of the five events sampled in this study and in agreement with previous work (Alibay, Burusco, et al. 2018), the $^4C_1$ to $^1C_4$ transition involves high energy intermediate steps, where the reducing GlcNAc ring adopts boat and skewed-

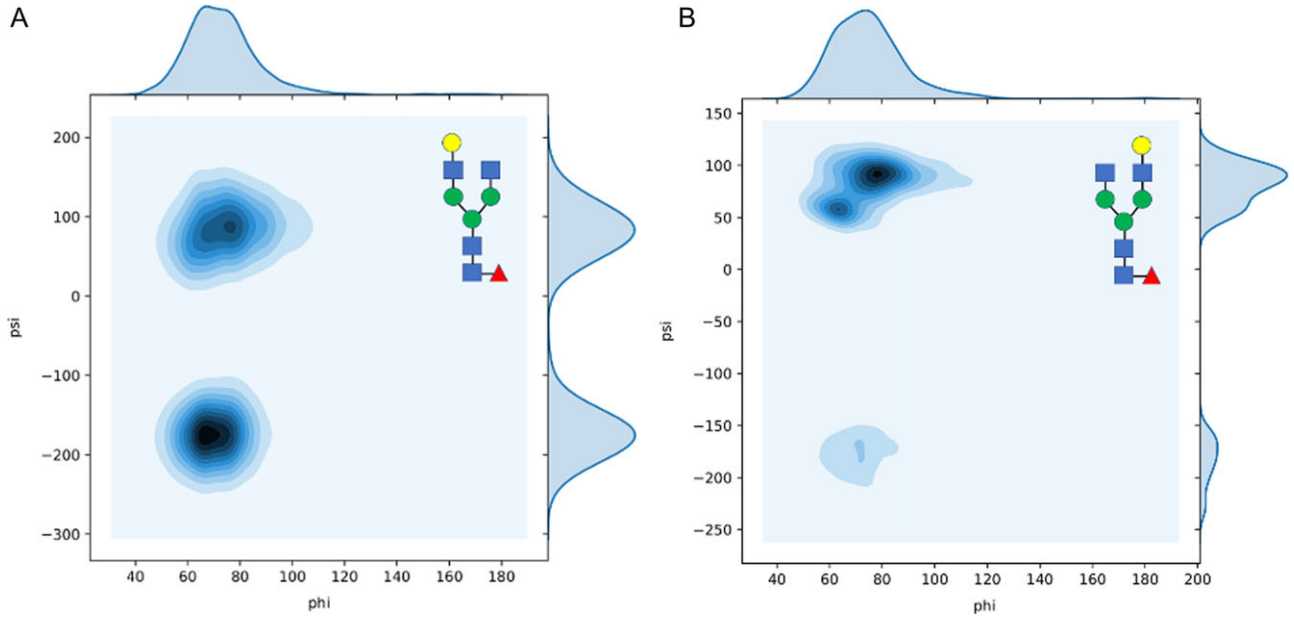

Fig. 7. Contour plot showing the different conformational propensities of the α(1–6) arm in sugar J (**A**) and L (**B**) in function of galactosylation. The "folded over" conformation corresponds to a ψ value around 80°, while the outstretched conformation corresponds to a ψ value around −180°. Torsion angles are in degrees. 2D contour plots are done with seaborn (*seaborn.pydata.org*) with 2500 data points.

boat conformations, while the β(1–4)-GlcNAc and the α(1–6)-Fuc change from an equatorial to an axial configuration. It is reasonable that the energy cost involved in this latter equatorial-to-axial conversion is less for the more flexible sugar D, relative to the more rigid (s)Le^x and (s)Le^a. The conformational propensity of the α(1–6) linkage through the 3 μs trajectory is shown in Figure S1.

Conclusions

Here we have shown the results of extensive sampling obtained through unbiased MD simulations of the conformational space accessible to increasingly larger biantennary complex *N*-glycans, commonly expressed at the Asn 297 in the IgG Fc region. Our data indicate that while core-fucosylation and sialylation do not affect the overall conformation of the isolated *N*-glycan as a whole, but contribute to its local dynamics, galactosylation of the α(1–6) arm shifts its conformational equilibrium towards a structure where the arm is "folded over" the chitobiose core. This effect is determined by more effective hydrogen bonding and stacking interactions between the chitobiose and the galactosylated α(1–6) arm and it is independent of the sequence of the α(1–3) arm, of core-fucosylation, and of sialylation of the α(1–6) arm. These results can explain the differential recognition of positional isomers (Echeverria, Serna, et al. 2018) and with the preference of sialyltransferases for the α(1–3) arm in both, isolated and Fc-linked *N*-glycans (Barb and Prestegard 2011). Currently we are in the process of determining how the dynamics and the conformational equilibria we have discussed here for the isolated biantennary *N*-glycans are affected by the presence of contacts with the IgG Fc protein surface. As a note, a relatively long simulation of the tetrasaccharide Man-β(1–4)-GlcNAc-β(1–4)-[α(1–6)-Fuc]-GlcNAc, named here sugar D, has highlighted an equilibrium between a high populated "closed" form of the sugar, where GlcNAc(1) is in the stable $^4C_1$ chair conformation, and an "open" form, where GlcNAc(1) is in the $^1C_4$ chair conformation. We find that the accessibility to the open state is significantly higher for sugar D, relative to (s)Le$^{x(a)}$, as reported in recent work (Topin, Lelimousin, et al. 2016; Alibay, Burusco, et al. 2018). This is most likely due to the higher flexibility of the α(1–6)-linked fucose relative to the α(1–3/4).

Computational methods

All glycans were built with the carbohydrate builder tool on GLYCAM-WEB (http://www.glycam.org). All combinations of rotamers for the α(1/2–6) linkages have been considered as starting structures for the MD simulations, namely 3 trajectories for one α(1–6) linkage, 9 for two α(1–6) linkages, 12 for one α(1–6) and one α(2–6) linkages, 24 for two α(1–6) and one α(2–6) linkages, and finally 72 for two α(1–6) and two α(2–6) linkages. Note, only less than 64 structures can be downloaded from the GLYCAM-WEB site. An overview of the systems size, in terms of atom numbers, and simulation times is shown in Table S1. The GLYCAM-06h-12SB version of the GLYCAM06 force field (Kirschner, Yongye, et al. 2008) was used to represent the carbohydrate atoms, TIP3P parameters (Jorgensen and Jenson 1998) were used to represent water, while amber99SB parameters (Hornak, Abel, et al. 2006) were used for the counterions, added in a number sufficient to neutralize the charge in the case of sialylated species. All simulations were run with versions 12 and 16 of the AMBER molecular simulation package (Salomon-Ferrer, Case, et al. 2013). Dispersion interactions were cutoff at a distance of 13 Å. Electrostatics interactions were treated with Particle Mesh Ewald (PME). A constant pressure of 1 atm was maintained by isotropic position scaling with a relaxation time of 2 ps, while a constant temperature of 300 K was regulated by Langevin dynamics using a collision frequency of 1.0 ps^{-1}. The SHAKE algorithm was used to restrain bonds with hydrogen atoms and an integration time step of 2 fs was used throughout. For each sugar, each starting structure was analyzed for at least 250 ns, with exceptions of sugar D, which was analyzed for 3 μs, because of the complexity of its dynamics, which will be discussed in the sections

below, and sugar E for 500 ns on single trajectories. Further details on the minimization, equilibration and production phases are included as Supplementary Material. As a note of warning, we have found that the direct translation of the GLYCAM/AMBER topology to GMX format with the AnteChamber PYthon Parser interfacE (*acpype.py*) (Sousa da Silva and Vranken 2012) can result in a misrepresentation of the torsion potentials, which affects primarily the conformation of the flexible (1/2–6) linkages. More information and test cases are included as Supplementary Material.

Supplementary data

Supplementary data is available at *Glycobiology* online.

Acknowledgements

E.F. would like to thank Dr Franck Fieschi (Institut de Biologie Structurale (IBS), Grenoble) for insightful discussions. The authors gratefully acknowledge the Irish Center for High-End Computing (ICHEC) for the generous allocation of computational resources. The John and Pat Hume Doctoral Awards program at Maynooth University is also gratefully acknowledged for funding.

Conflict of interest statement

None declared.

Abbreviations

ADCC, antibody-dependent cell-mediated cytotoxicity; Fc, fragment crystallizable; FcγRIIIa, Fc γ receptor IIIa; GFDB, glycan fragment database; IgGs, immunoglobulins G; PME, Particle Mesh Ewald.

References

Alibay I, Burusco KK, Bruce NJ, Bryce RA. 2018. Identification of rare lewis oligosaccharide conformers in aqueous solution using enhanced sampling molecular dynamics. *J Phys Chem B*. 122:2462–2474.

Anthony RM, Nimmerjahn F, Ashline DJ, Reinhold VN, Paulson JC, Ravetch JV. 2008. Recapitulation of IVIG anti-inflammatory activity with a recombinant IgG Fc. *Science*. 320:373–376.

Arnold JN, Wormald MR, Sim RB, Rudd PM, Dwek RA. 2007. The impact of glycosylation on the biological function and structure of human immunoglobulins. *Annu Rev Immunol*. 25:21–50.

Barb AW, Brady EK, Prestegard JH. 2009. Branch-specific sialylation of IgG-Fc glycans by ST6Gal-I. *Biochemistry*. 48:9705–9707.

Barb AW, Prestegard JH. 2011. NMR analysis demonstrates immunoglobulin G N-glycans are accessible and dynamic. *Nat Chem Biol*. 7:147–153.

Canales A, Mallagaray A, Perez-Castells J, Boos I, Unverzagt C, Andre S, Gabius HJ, Canada FJ, Jimenez-Barbero J. 2013. Breaking pseudo-symmetry in multiantennary complex N-glycans using lanthanide-binding tags and NMR pseudo-contact shifts. *Angew Chem Int Ed Engl*. 52: 13789–13793.

Chen CL, Hsu JC, Lin CW, Wang CH, Tsai MH, Wu CY, Wong CH, Ma C. 2017. Crystal structure of a homogeneous IgG-Fc glycoform with the N-glycan designed to maximize the antibody dependent cellular cytotoxicity. *ACS Chem Biol*. 12:1335–1345.

de Jong SE, Selman MHJ, Adegnika AA, Amoah AS, van Riet E, Kruize YCM, Raynes JG, Rodriguez A, Boakye D, von Mutius E et al. 2016. IgG1 Fc N-glycan galactosylation as a biomarker for immune activation. *Sci Rep*. 6:28207.

Echeverria B, Serna S, Achilli S, Vives C, Pham J, Thepaut M, Hokke CH, Fieschi F, Reichardt NC. 2018. Chemoenzymatic synthesis of N-glycan positional isomers and evidence for branch selective binding by monoclonal antibodies and human C-type lectin receptors. *ACS Chem Biol*. 13:2269–2279.

Fang J, Richardson J, Du ZM, Zhang ZQ. 2016. Effect of Fc-glycan structure on the conformational stability of IgG revealed by hydrogen/deuterium exchange and limited proteolysis. *Biochemistry*. 55:860–868.

Ferrara C, Grau S, Jager C, Sondermann P, Brunker P, Waldhauer I, Hennig M, Ruf A, Rufer AC, Stihle M et al. 2011. Unique carbohydrate-carbohydrate interactions are required for high affinity binding between FcgammaRIII and antibodies lacking core fucose. *Proc Natl Acad Sci USA*. 108:12669–12674.

Galvelis R, Re S, Sugita Y. 2017. Enhanced conformational sampling of N-glycans in solution with replica state exchange metadynamics. *J Chem Theory Comput*. 13:1934–1942.

Gudelj I, Salo PP, Trbojevic-Akmacic I, Albers M, Primorac D, Perola M, Lauc G. 2018. Low galactosylation of IgG associates with higher risk for future diagnosis of rheumatoid arthritis during 10 years of follow-up. *Biochim Biophys Acta*. 1864:2034–2039.

Hayes JM, Frostell A, Karlsson R, Muller S, Millan-Martin S, Pauers M, Reuss F, Cosgrave E, Anneren C, Davey GP et al. 2017. Identification of Fc gamma receptor glycoforms that produce differential binding kinetics for rituximab. *Mol Cell Proteomics*. 16:1770–1788.

Hornak V, Abel R, Okur A, Strockbine B, Roitberg A, Simmerling C. 2006. Comparison of multiple amber force fields and development of improved protein backbone parameters. *Proteins*. 65:712–725.

Iida S, Kuni-Kamochi R, Mori K, Misaka H, Inoue M, Okazaki A, Shitara K, Satoh M. 2009. Two mechanisms of the enhanced antibody-dependent cellular cytotoxicity (ADCC) efficacy of non-fucosylated therapeutic antibodies in human blood. *BMC Cancer*. 9:58.

Iida S, Misaka H, Inoue M, Shibata M, Nakano R, Yamane-Ohnuki N, Wakitani M, Yano K, Shitara K, Satoh M. 2006. Nonfucosylated therapeutic IgG1 antibody can evade the inhibitory effect of serum immunoglobulin g on antibody-dependent cellular cytotoxicity through its high binding to Fc gamma RIIIa. *Clin Cancer Res*. 12:2879–2887.

Jo S, Im W. 2013. Glycan fragment database: A database of PDB-based glycan 3D structures. *Nucleic Acids Res*. 41:D470–D474.

Jo S, Lee HS, Skolnick J, Im W. 2013. Restricted N-glycan conformational space in the PDB and its implication in glycan structure modeling. *PLoS Comput Biol*. 9:e1002946.

Jo S, Qi YF, Im W. 2016. Preferred conformations of N-glycan core pentasaccharide in solution and in glycoproteins. *Glycobiology*. 26:19–29.

Jorgensen WL, Jenson C. 1998. Temperature dependence of TIP3P, SPC, and TIP4P water from NPT Monte Carlo simulations: Seeking temperatures of maximum density. *J Comp Chem*. 19:1179–1186.

Kanda Y, Yamada T, Mori K, Okazaki A, Inoue M, Kitajima-Miyama K, Kuni-Kamochi R, Nakano R, Yano K, Kakita S et al. 2007. Comparison of biological activity among nonfucosylated therapeutic IgG1 antibodies with three different N-linked Fc oligosaccharides: The high-mannose, hybrid, and complex types. *Glycobiology*. 17:104–118.

Karsten CM, Pandey MK, Figge J, Kilchenstein R, Taylor PR, Rosas M, McDonald JU, Orr SJ, Berger M, Petzold D et al. 2012. Anti-inflammatory activity of IgG1 mediated by Fc galactosylation and association of FcgammaRIIB and dectin-1. *Nat Med*. 18:1401–1406.

Kirschner KN, Yongye AB, Tschampel SM, Gonzalez-Outeirino J, Daniels CR, Foley BL, Woods RJ. 2008. GLYCAM06: A generalizable biomolecular force field. Carbohydrates. *J Comp Chem*. 29:622–655.

Kobata A. 2008. The N-linked sugar chains of human immunoglobulin G: Their unique pattern, and their functional roles. *Biochim Biophys Acta*. 1780:472–478.

Krapp S, Mimura Y, Jefferis R, Huber R, Sondermann P. 2003. Structural analysis of human IgG-Fc glycoforms reveals a correlation between glycosylation and structural integrity. *J Mol Biol*. 325:979–989.

Lee HS, Im W. 2017. Effects of N-glycan composition on structure and dynamics of IgG1 Fc and their implications for antibody engineering. *Sci Rep*. 7:12659.

Li T, DiLillo DJ, Bournazos S, Giddens JP, Ravetch JV, Wang LX. 2017. Modulating IgG effector function by Fc glycan engineering. *Proc Natl Acad Sci U S A*. 114:3485–3490.

Matsumiya S, Yamaguchi Y, Saito J, Nagano M, Sasakawa H, Otaki S, Satoh M, Shitara K, Kato K. 2007. Structural comparison of fucosylated and nonfucosylated Fc fragments of human immunoglobulin G1. *J Mol Biol*. 368:767–779.

Oflazoglu E, Audoly LP. 2010. Evolution of anti-CD20 monoclonal antibody therapeutics in oncology. *MAbs*. 2:14–19.

Okazaki A, Shoji-Hosaka E, Nakamura K, Wakitani M, Uchida K, Kakita S, Tsumoto K, Kumagai I, Shitara K. 2004. Fucose depletion from human IgG1 oligosaccharide enhances binding enthalpy and association rate between IgG1 and Fc gamma RIIIa. *J Mol Biol*. 336:1239–1249.

Parekh RB, Dwek RA, Sutton BJ, Fernandes DL, Leung A, Stanworth D, Rademacher TW, Mizuochi T, Taniguchi T, Matsuta K et al. 1985. Association of rheumatoid arthritis and primary osteoarthritis with changes in the glycosylation pattern of total serum IgG. *Nature*. 316:452–457.

Parekh R, Isenberg D, Rook G, Roitt I, Dwek R, Rademacher T. 1989. A comparative analysis of disease-associated changes in the galactosylation of serum IgG. *J Autoimmun*. 2:101–114.

Pasek M, Duk M, Podbielska M, Sokolik R, Szechinski J, Lisowska E, Krotkiewski H. 2006. Galactosylation of IgG from rheumatoid arthritis (RA) patients—Changes during therapy. *Glycoconjugate J*. 23:463–471.

Pucic M, Knezevic A, Vidic J, Adamczyk B, Novokmet M, Polasek O, Gornik O, Supraha-Goreta S, Wormald MR, Redzic I et al. 2011. High throughput isolation and glycosylation analysis of IgG-variability and heritability of the IgG glycome in three isolated human populations. *Mol Cell Proteomics*. 10:M111.010090.

Raju TS. 2008. Terminal sugars of Fc glycans influence antibody effector functions of IgGs. *Curr Opin Immunol*. 20:471–478.

Raju TS, Briggs JB, Borge SM, Jones AJS. 2000. Species-specific variation in glycosylation of IgG: Evidence for the species-specific sialylation and branch-specific galactosylation and importance for engineering recombinant glycoprotein therapeutics. *Glycobiology*. 10:477–486.

Ratner M. 2014. Genentech's glyco-engineered antibody to succeed Rituxan. *Nat Biotechnol*. 32:6–7.

Salomon-Ferrer R, Case DA, Walker RC. 2013. An overview of the Amber biomolecular simulation package. *WIREs Comput Mol Sci*. 3:198–210.

Satoh M, Iida S, Shitara K. 2006. Non-fucosylated therapeutic antibodies as next-generation therapeutic antibodies. *Expert Opin Biol Ther*. 6: 1161–1173.

Sehnal D, Deshpande M, Varekova RS, Mir S, Berka K, Midlik A, Pravda L, Velankar S, Koca J. 2017. LiteMol suite: Interactive web-based visualization of large-scale macromolecular structure data. *Nat Methods*. 14: 1121–1122.

Shields RL, Namenuk AK, Hong K, Meng YG, Rae J, Briggs J, Xie D, Lai J, Stadlen A, Li B et al. 2001. High resolution mapping of the binding site on human IgG1 for Fc gamma RI, Fc gamma RII, Fc gamma RIII, and FcRn and design of IgG1 variants with improved binding to the Fc gamma R. *J Biol Chem*. 276:6591–6604.

Sousa da Silva AW, Vranken WF. 2012. ACPYPE—AnteChamber PYthon Parser interfacE. *BMC Res Notes*. 5:367.

Strohl WR. 2009. Optimization of Fc-mediated effector functions of monoclonal antibodies. *Curr Opin Biotechnol*. 20:685–691.

Subedi GP, Barb AW. 2016. The immunoglobulin G1 N-glycan composition affects binding to each low affinity Fc gamma receptor. *MAbs*. 8: 1512–1524.

Tao MH, Morrison SL. 1989. Studies of aglycosylated chimeric mouse-human IgG. Role of carbohydrate in the structure and effector functions mediated by the human IgG constant region. *J Immunol*. 143: 2595–2601.

Topin J, Lelimousin M, Arnaud J, Audfray A, Perez S, Varrot A, Imberty A. 2016. The hidden conformation of Lewis x, a human histo-blood group antigen, is a determinant for recognition by pathogen lectins. *ACS Chem Biol*. 11:2011–2020.

van den Eijnden DH, Joziasse DH, Dorland L, van Halbeek H, Vliegenhart JFG, Schmid K. Specificity in the enzymic transfer of sialic acid to the oligosaccharide branches of BI- and triantennary glycopeptides of alpha1-acid glycoprotein. *Biochem Biophys Res Comm*. 92(3): 839–845.

Varki A, Cummings RD, Aebi M, Packer NH, Seeberger PH, Esko JD, Stanley P, Hart G, Darvill A, Kinoshita T et al. 2015. Symbol Nomenclature for graphical representation of glycans. *Glycobiology*. 25(12): 1323–1324.

Wormald MR, Petrescu AJ, Pao YL, Glithero A, Elliott T, Dwek RA. 2002. Conformational studies of oligosaccharides and glycopeptides: Complementarity of NMR, X-ray crystallography, and molecular modelling. *Chem Rev*. 102:371–386.